Journal of Electronic Materials (2022) 51:2346–2355
https://doi.org/10.1007/s11664-022-09479-w

ORIGINAL RESEARCH ARTICLE

The Structural, Electronic, Magnetic, and Optical Properties of CsTe Monolayer: Effects of the Biaxial Strain and Electrical Field

Jabbar M. Khalaf Al-zyadi[1] · Ahmed Hamad Ati[1] · Ammar A. Kadhim[2] · Furat A. Al-Saymari[1]

Received: 4 August 2021 / Accepted: 24 January 2022 / Published online: 25 February 2022

Abstract

Herein we report intrinsic ferromagnetism in a two-dimensional layer for the hexagonal monolayer of CsTe based on first-principles calculations. The aim of this work is to explore the structural, electronic, magnetic, and optical properties of the monolayer of CsTe. To achieve this goal, we systematically investigate the effect of biaxial strain and electric field on the electronic and magnetic properties of the CsTe. Monolayer CsTe has a half metallic (HM) property, and the magnitude of the magnetic moment is equal to 1 μ_B for each unit cell. Under the influence of biaxial strain, the size of the energy gap in the spin-up channel decreases under tensile strain and increases under compressive strain. The magnetic moment values show no change, and therefore, the HM behavior can be maintained for larger strains. The electric field has a clear effect on the energy gap when the electric field increases to $E = -0.6$ V/nm, which destroys the HM characteristic since the magnetic moment of the Cs is increased far more than the Te moment, and the Te has a large effect on achieving the HM property. The calculated optical properties indicate that the investigated material is a good candidate for applications related to microelectronic and optoelectronic devices.

Keywords First-principles study · CsTe monolayer · optical properties · biaxial strain · electric field

Introduction

Spintronics is a promising technology for the development of the next generation of information technology due to its impressive characteristics in transmitting information and energy consumption. The materials used in the manufacturing of these devices require high spin polarization (SP) for the sake of improving their efficiency and utility. Among the most important applications are the spin valve, the spin filter, and the spin diode.[1–3] Half-metallic (HM) materials are most desirable in the manufacturing of spintronic devices, as they carry high spin polarization equal to 100% for the spin of the electrons at the Fermi level and have two different spin channels, i.e., ↑ and ↓. One is conductive, and the other is either semiconducting or insulating depending on the width of the energy gap.[4] So far, HM materials have been employed in a three-dimensional (3D) compound form, such as Heusler alloys,[5] transition-metal pnictides and chalcogenides,[6] double perovskites,[7] and transition-metal oxides.[8–10] The HM property in the practical measurements of compounds is usually verified using spin-resolved photoelectron spectroscopy,[9] spin-polarized electron tunneling,[11] and Andreev reflection.[10,12] In recent years, researchers have increased their interest theoretically and practically to describe and prepare two-dimensional (2D) materials, especially since the discovery of graphene,[13] borophene,[14] hexagonal boron nitride *h*-BN,[15] and transition metal dichalcogenides.[16] Despite the rapid expansion of the family of 2D materials, a ferromagnetic HM nanosheet is still missing. The existence of 2D HM materials remains controversial from an experimental point of view, despite the existence of several theoretical studies that describe the properties of the HM materials representing a 2D compound.

In the bulk structure, the metal monochalcogenides (such as GaS, GaSe, InSe, and GaTe) are layered materials consisting of metal and chalcogen atoms linked by a covalent bond with nanometer-thick layers coupled by weak ionic bonds and van der Waal forces.[17] Like graphene, these materials can be diluted to form 2D crystals. This state can be

✉ Jabbar M. Khalaf Al-zyadi
jabbar.khalaf@uobasrah.edu.iq; jabbar_alzyadi@yahoo.com

[1] Department of Physics, College of Education for Pure Sciences, University of Basrah, Basrah, Iraq

[2] Department of Chemistry, College of Education/Qurna, University of Basrah, Basrah, Iraq

generalized to suit the compound used in the current study, which is CsTe. It is known that in 2D materials, the magnetization is highly dependent on the number of layers, contrary to the bulk structure (3D).[18,19] This was observed in the study of the VSe_2 compound, which is in the paramagnetic state at 3D and the ferromagnetic state at 2D.[20–23]

There are many 2D compounds with an HM characteristic. The most important of these compounds are CrX (X = P, As, Sb),[24] Na_2C,[25] and YN_2 which has a Dirac HM feature.[26] The optical properties, strain effect, electric field, and thermoelectric nature of 2D materials have attracted vast research efforts due to their splendid characteristics.[27–36] Many studies have been conducted on the surface and interfacial properties of HM materials, most of which do not preserve HM properties on surfaces and interfaces.[37–40]

In this paper, CsTe in the form of a 2D compound will be discussed, as it has been previously studied in 3D form and at surfaces.[41] We organized our paper in such a way that it firstly includes the mathematical and theoretical details. Secondly, it includes a discussion of the atomic structure and the electronic and magnetic properties of pristine monolayer CsTe. Finally, it examines the biaxial strain and the electric field by studying their effects on the electronic, magnetic, and optical properties. By analyzing the density of states and magnetic moment, the aim is to find CsTe material in the monolayer form which can be used in spintronic devices. The results indicate that CsTe monolayer is a promising candidate for 2D spintronic applications.

Computational Method

To calculate the structural, electronic, magnetic, and optical properties of CsTe, density functional theory (DFT) was used and applied to the CASTEP code.[42] The exchange–correlation energy has been treated depending on the generalized gradient approximation (GGA) with the Perdew–Burke–Ernzerhof (PBE) formulation.[43] The model system built is the CsTe monolayer which consists of a $4 \times 4 \times 1$ supercell with the addition of 15 Å in the direction perpendicular to the 2D monolayer surface to eliminate artificial interactions that might exist between the rotating images of the panels along the vertical direction. Additionally, the initial spin configurations of CsTe are evaluated depending on spin results, nonmagnetic (no spin), ferromagnetic (spin in one direction, up or down, and the material has magnetic moment), and antiferromagnetic (spin up = spin down, and the magnetic moments is zero), indicating that the CsTe is ferromagnetic. In the calculations, a separation power of 300 eV on a plan-wave basis is used, and all structures are completely at rest with a force acting on the atoms lower than 0.01 eV/Å, and the total energy convergence is 10^{-6} eV. The first Brillouin region is sampled by a k-mesh ($15 \times 15 \times 1$) to simulate the structural, electronic, magnetic, and optical properties of the CsTe monolayer. The biaxial strain and electric field are applied to the CsTe monolayer ranging from +6% to −6% and +0.6 V/nm to −0.6 V/nm, respectively.

Results and Discussion

Pristine Monolayer CsTe

The atomic structure of the monolayer CsTe has a P3m1 (no. 156) space group, and the geometric shape of this compound consists of two Cs and Te atoms, as shown in Fig. 1a. Firstly, the geometric structure is improved by considering all the atoms in a relaxed state. The crystal lattice constant is determined and found to be equal to 6.346 Å, and the bond length of Cs–Te is 3.689 Å. The CsTe monolayer is not a completely flat structure, i.e., has buckling between Cs and Te atoms. The charge density of the difference is

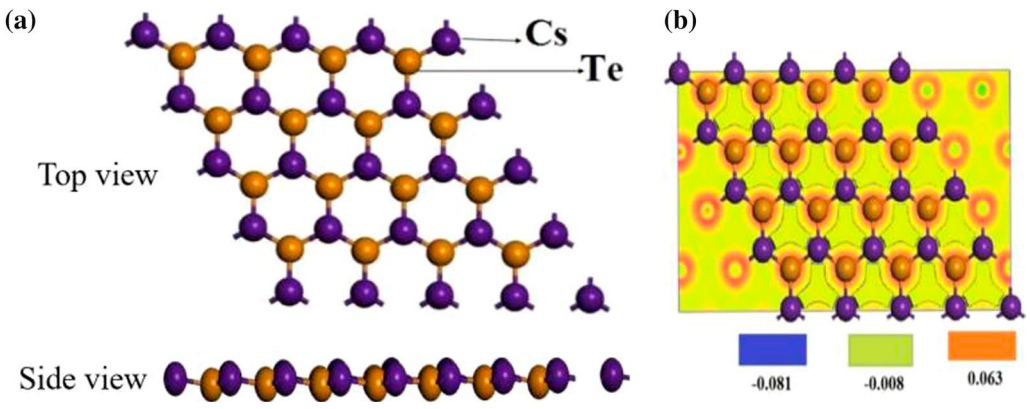

Fig. 1 (a) Top and side view of the atomic structure of CsTe monolayer. The orange and blue dots are Cs and Te atoms, respectively. (b) The difference in charge density for monolayer CsTe in units of $e/Å^3$ (Color figure online).

calculated by subtracting the charge density of the free Cs and Te atoms from the total charge density of CsTe; see Fig. 1b. The orange region shows that charges accumulated at Te, while there is an attenuation of charges at Cs in the blue region. The negatively charged Te atoms are surrounded by positively charged Cs atoms, which is evidence of charge transfer from Cs atoms to Te atoms.

To study the electronic properties, the electronic band structure, total density of states (TDOS), and partial density of states (PDOS) are shown in Fig. 2a and b. The results indicate that CsTe monolayer is HM with SP = 100%, where the spin ↓ channel is metallic, and the spin ↑ channel is a semiconductor with an indirect energy gap equal to 2.441 eV. The valence band maximum (VBM) is located at the *K* point, and conduction band minimum (CBM) is located at the *G* point, while the half-metallic gap (HM_{Gap}) is 0.111eV, which is calculated from the Fermi level to the VBM.

The contribution of Te element is effective since this element holds six electrons, two in the *s* orbital and four in the *p* orbital, and the electrons are the ones that have passed the Fermi level. Therefore, the contribution of Te is greater than Cs since the magnetic moment for Te is 1.03 μ_B, while it is equal to −0.03 μ_B for Cs because of its high electronegativity (see Fig. 2c and d). This spin distribution corresponds to the parallel orientation of the monolayer atoms; hence, the monolayer has ferromagnetic properties. Ultimately, the total magnetic moment was estimated to be 16 μ_B at the ground state for the monolayer CsTe, while it is 1 μ_B for each unit cell. For half metals, the total magnetic moment is equal to integers.[44]

Biaxial Strain Effect

Strain engineering is currently a good way to modify the electronic properties of 2D materials, so it is interesting to demonstrate these effects on the monolayer of CsTe. Consider the effect of a biaxial strain (S_b) on electronic and magnetic properties. A biaxial strain is defined as

$$S_b = \Delta a/a_o \times 100\%,\ \Delta a = a \pm a_o \quad (1)$$

where a and a_o are strained and nonstrained lattice constants, respectively. The positive sign refers to the tensile strain, and the negative sign to the compressive strain. The S_b is implemented along the *x*–*y* axis. The density of states and electronic band structure under the S_b are shown in Figs. 3 and 4, respectively. It is found that the lattice constants and bond lengths increase under $S_b > 0$ and decrease at $S_b < 0$. We have also found that the monolayer bears an HM property in all cases under of the effect of S_b, so the spin ↑ channel is semiconducting, while the spin ↓ channel is metallic. The effect of S_b is evident in the energy gap in the spin ↑ channel.

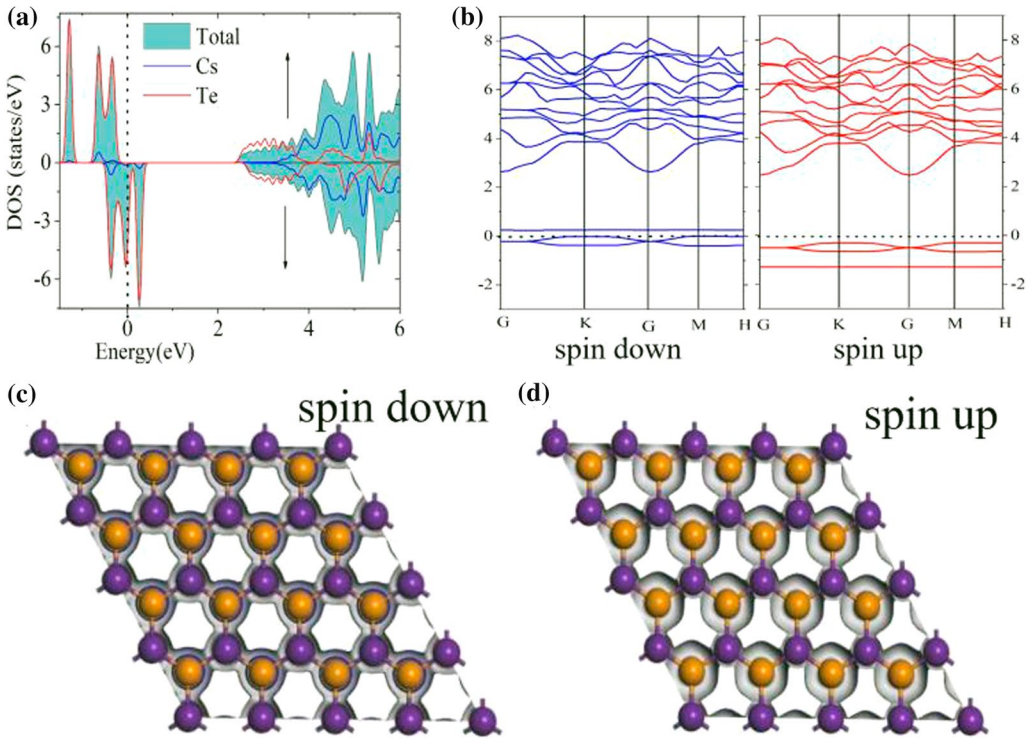

Fig. 2 (a) The densities of states of monolayer CsTe. (b) Band structure of the minority (spin ↓) and majority (spin ↑) CsTe. (c, d) The difference in spin density distributions of spin ↓ and spin ↑ states, respectively.

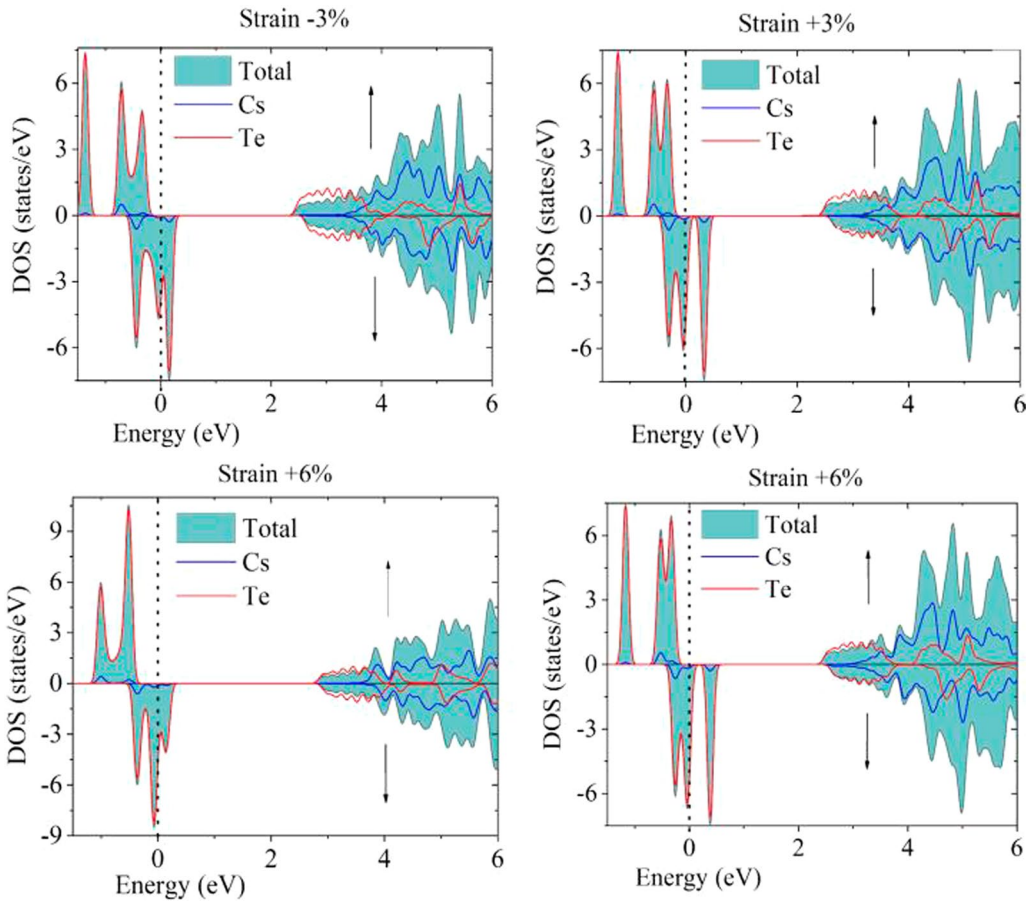

Fig. 3 The density of states of monolayer CsTe under the biaxial strain.

It is noticed that under the biaxial tensile strain, the VBM and CBM continuously shift toward the Fermi level, so that the energy gap decreases in the tensile strain from 2.431 eV in $S_b = +3\%$ to 2.409 eV in $S_b = +6\%$, while it increases at the compressive strain, and the VBM and CBM constantly shift away from the Fermi level, viz., from 2.463 eV in $S_b = -3\%$ to 2.968 eV in $S_b = -6\%$. These results show that as the coefficient of the lattice constant increases, the energy gap decreases and vice versa,[45] as is clear in Fig. 5a.

Conducting the Mulliken analysis, it is discovered that when monolayer CsTe is under biaxial strain, the magnetic moment values are constant under the tensile strain and also under the compressive strain. As such, both Cs and Te atoms are equal to −0.03 and 1.03 μ_B, respectively. Thus the total magnetic moment is equal to 1 μ_B. These results lead to the conclusion that the magnetic moment cannot be modified under the influence of the strain for monolayer CsTe.

Electric Field Effect

The influence of an external electric field (E) on the electronic and magnetic properties of the monolayer CsTe can be studied by applying a perpendicular E to the plane of the monolayer CsTe. Initially, the direction of the applied E was perpendicular to the positive direction of the z-axis. Next, the direction of the E was reversed in the negative direction of the z-axis. The density of states and electronic band structure under E effect show that the energy gap changes from indirect to direct, as is clear in Figs. 6 and 7, respectively.

In addition, it is found that the CsTe compound at $E = +0.3$ V /nm is HM ferromagnetic, so that the spin ↑ channel becomes semiconducting with an energy gap equal to 0.613 eV, while the spin-down channel is metallic. When the $E = -0.3$ V/nm and the occupation spin channels change, the spin ↑ channel turns metallic, and the spin ↓ channel becomes semiconducting with a gap equal to 2.790 eV. This situation is due to the increase in the charge carriers of the Cs atom because when the E is applied, the positive Cs charges move toward the negative charge Te region. The converse is true for negative charges, which move toward the positively charged region.

However, when $E = +0.6$ V/nm, an overlap occurs between the VBM and CBM, and as a result, the HM property is destroyed. Finally, when $E = -0.6$ V/nm it turns out that it is

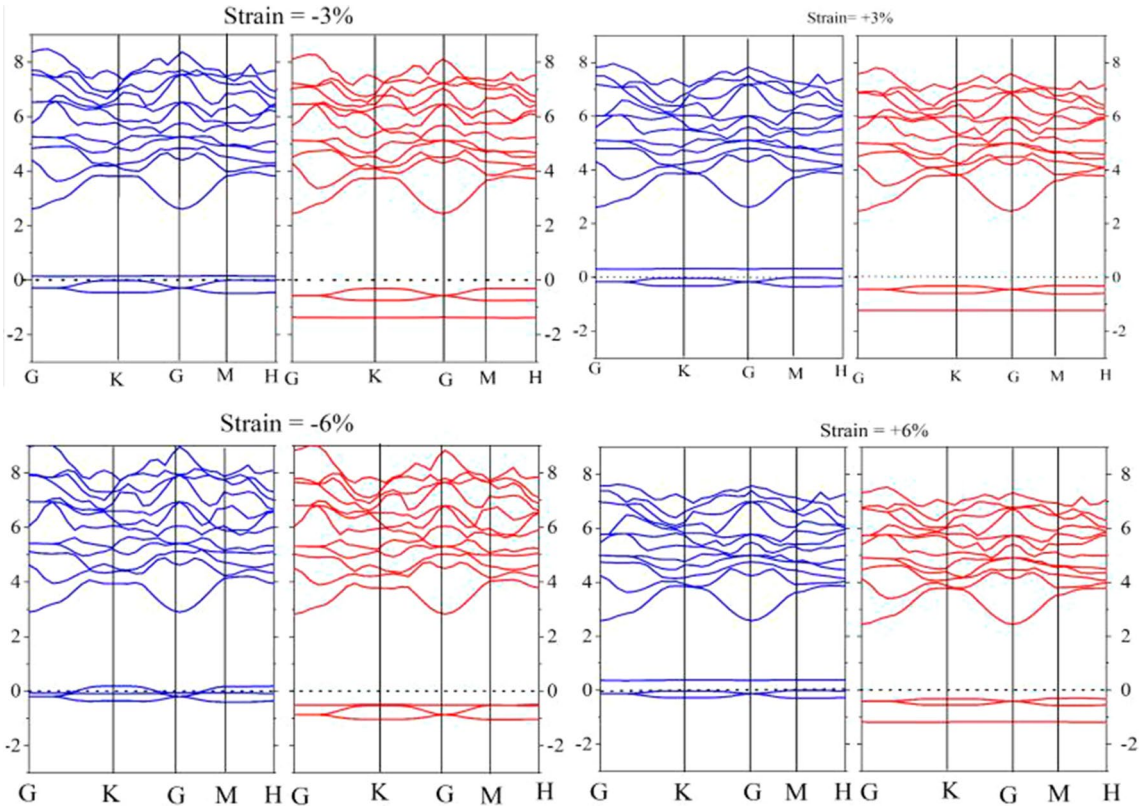

Fig. 4 Electronic band structure of CsTe as a function of biaxial strains; red line (spin down) and blue line (spin up). The zero energy is set to E_F (Color figure online).

a semiconductor with an energy gap of (0.314 eV), and here the magnitude of the SP is equal to 0. The change in the energy gap under the E effect appears in Fig. 5b.

We explore an important feature about the effect of the E on the magnetic properties based on the Mulliken analysis of the monolayer CsTe. It turns out that the magnetic moment of Cs and Te increases (decreases) with the increase in the E in both the positive and negative directions (see Table I). The magnitude of the magnetic moment of Cs increases due to the fact that the spin splitting increases as shown in the density of states in Fig. 6.

Optical Properties

Since CsTe is a semiconductor in the spin ↑ channel, it is important to investigate its optical manifestations. The optical properties of the CsTe monolayer were determined under S_b and E in the energy range 0–15 eV. The current study focuses on the basic optical properties such as the important dielectric function $\varepsilon(\omega)$, absorption coefficient $A(\omega)$, and optical $R(\omega)$ reflectivity. The dielectric function $\varepsilon(\omega)$ is given by

$$\varepsilon(\omega) = \varepsilon_1(\omega) + i\varepsilon_2(\omega) \tag{2}$$

where $\varepsilon_1(\omega)$ and $\varepsilon_2(\omega)$ are the imaginary and real parts of $\varepsilon(\omega)$, respectively. The dielectric function reflects the material response to E. The band structure plays an important role in describing the dielectric function, in that the dielectric function entirely depends on the occupied and unoccupied wave functions obtained by calculating the momentum matrix elements. The propagative behavior of the electromagnetic field is related to the real part $\varepsilon_1(\omega)$. The $\varepsilon_1(\omega)$ is derived from the Kramer–Kronig relation,[46] and the relationship for the imaginary part $\varepsilon_2(\omega)$ is obtained by summing the occupied–unoccupied transitions using the Fermi golden rule.[47]

As shown in Fig. 8, there was no peak for the real part at S_b and E; also, the results indicate that the monolayer CsTe is metallic at $E = -0.6$ V/nm because $\varepsilon_1(\omega)$ has a negative value. As for the imaginary part $\varepsilon_2(\omega)$, there is one peak for $S_b = 0\%$ at 1.73 (5.7 eV) and two peaks for $S_b = -6\%$ appeared; one of them is at 5.41 (0.98 eV) in the infrared (IR) region, and the other at 2.13 (5.13 eV) in the ultraviolet (UV) region, as is clear in Fig. 8a. The situation differs at E, where at each value of the E, a peak appears which can be determined within the photon energy range of 0.17–0.56 eV in the IR region; see Fig. 8b.

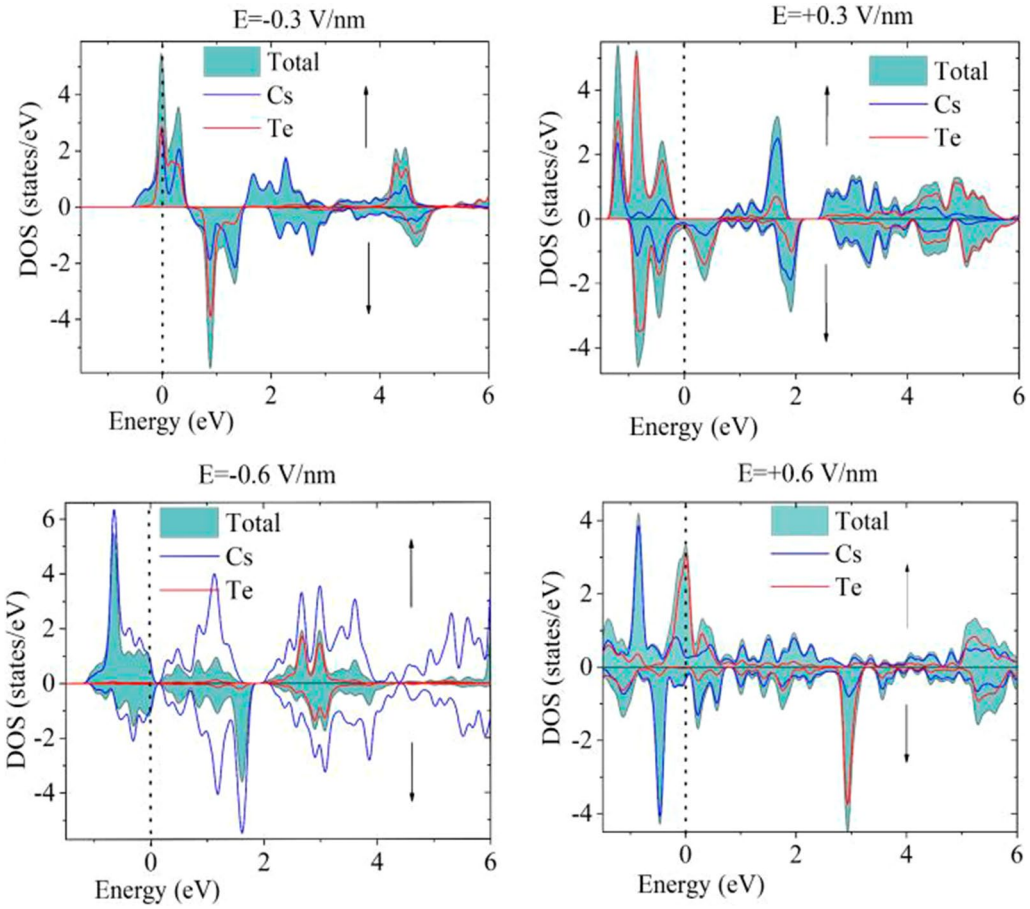

Fig. 5 The density of states of monolayer CsTe under an electric field effect.

To study the effect of S_b and E on the absorption coefficient $A(\omega)$, see Fig. 9a. In the case of $S_b = 0$ at (6.34 eV), the maximum $A(\omega)$ is 8.12×10^4 cm^{-1}. The compressive $S_b < 0$ moves the main optical absorption peak to the higher-energy region, while this peak is pushed down to the lower-energy domain in the case of the tensile strain $S_b > 0$. For $S_b = -6\%$, there is a peak in the IR region at 1.22 eV where $A(\omega) = 1.83 \times 10^4$ cm^{-1}. The change in the $A(\omega)$ values happened due to the change in the E at $E = -0.6$ V/nm, which has three peaks where $A(\omega) = 7.11 \times 10^4$ cm^{-1} is in the visible region, and the other two are in the UV region. As shown in Fig. 9b, the optical reflectivity $R(w)$ is very high in the UV light region and strongly dependent on S_b and E. The maximum optical $R(w)$ at equilibrium $S_b = 0$ is 15.09% in the UV region (7.08 eV). The ability to increase the absorption density of the CsTe monolayer by strain engineering, especially in the visible light region, is a very important point, which could open possibilities for its application in optical electronic devices. Regarding the electric field at $E = -0.6$ V/nm, the maximum value of the reflectivity is 74.32% at the visible region.

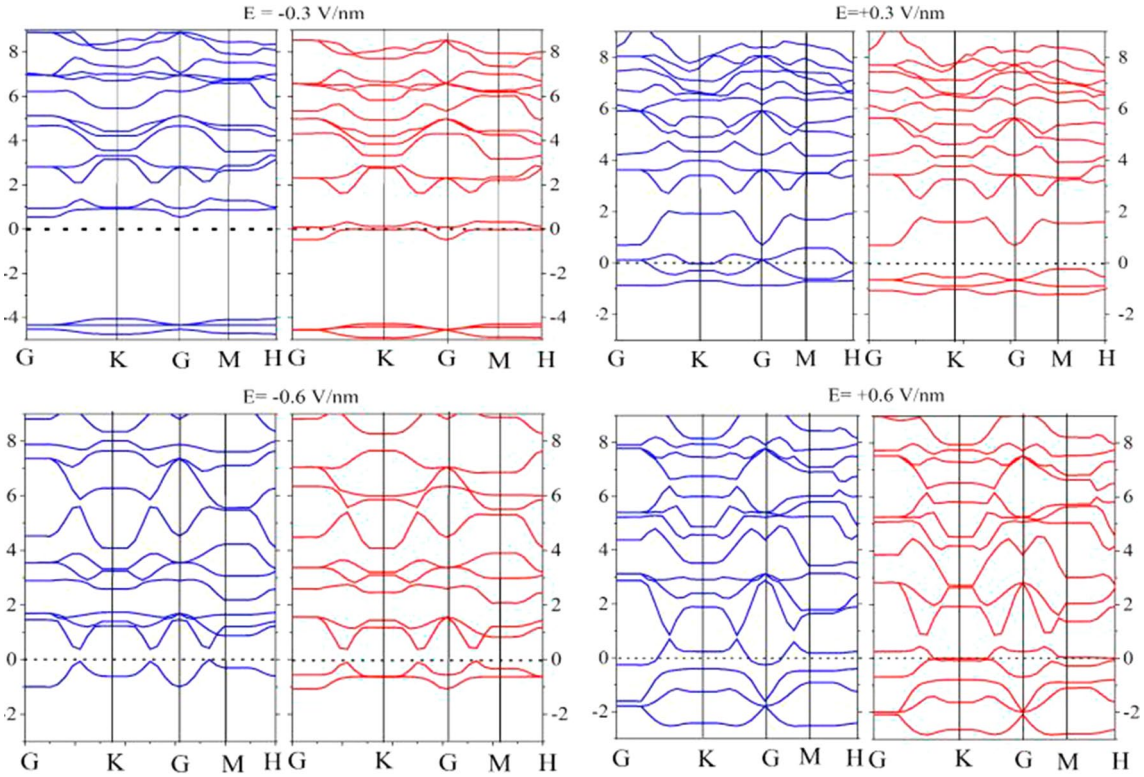

Fig. 6 Electronic band structure of monolayer CsTe as a function of electric field. The perpendicular electric field denotes parallel to the z-axis; the red line indicates spin down, and the blue line indicates spin up. The zero energy is set to E_F (Color figure online).

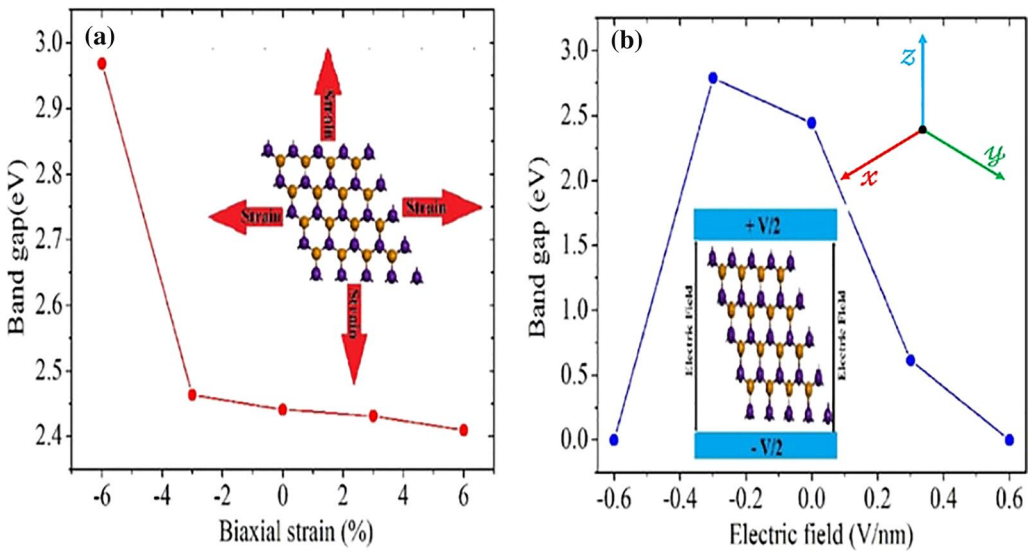

Fig. 7 Calculated band gap of CsTe monolayer as a function of (a) biaxial strain and (b) external electric field.

Conclusion

The effects of the biaxial strain and electric field on the structural, electronic, magnetic, and optical properties of a monolayer compound were systematically investigated using first-principles calculations. It is proved that CsTe is an HM ferromagnetic compound with a metallic property in the spin ↓ channel and a semiconductor in the spin ↑ channel with an indirect energy gap equal to 2.441 eV. It is found that the magnitude of the magnetic moment is equal to 1 μ_B and the energy gap is indirect, where it decreases with $S_b > 0$ and increases with $S_b < 0$. In all cases, the compound preserves the HM property. Moreover, when E is perpendicularly applied to the CsTe monolayer, the energy gap decreases until it fades with the increase in the E, and thus the HM property disappears at $E = -0.6$ V/nm. In addition, the magnetic moment of the Cs increases with the increase in E while it decreases with respect to the increase in Te. The effect of S_b in terms of optical properties is stronger than that of E. The wide absorption spectrum and the ability to control the absorption density by using S_b and E are very good, so that the monolayer has potential for applications in optical electronic devices.

Table I Calculation of magnetic moment in μ_B under the influence of an electric field within a range of +0.6 to −0.6 V/nm

Atom	$E = +0.3$ V/nm	$E = -0.3$ V/nm	$E = +0.6$ V/nm	$E = -0.6$ V/nm
Cs	0.24	0.44	0.43	0.98
Te	0.76	0.56	0.57	0.02

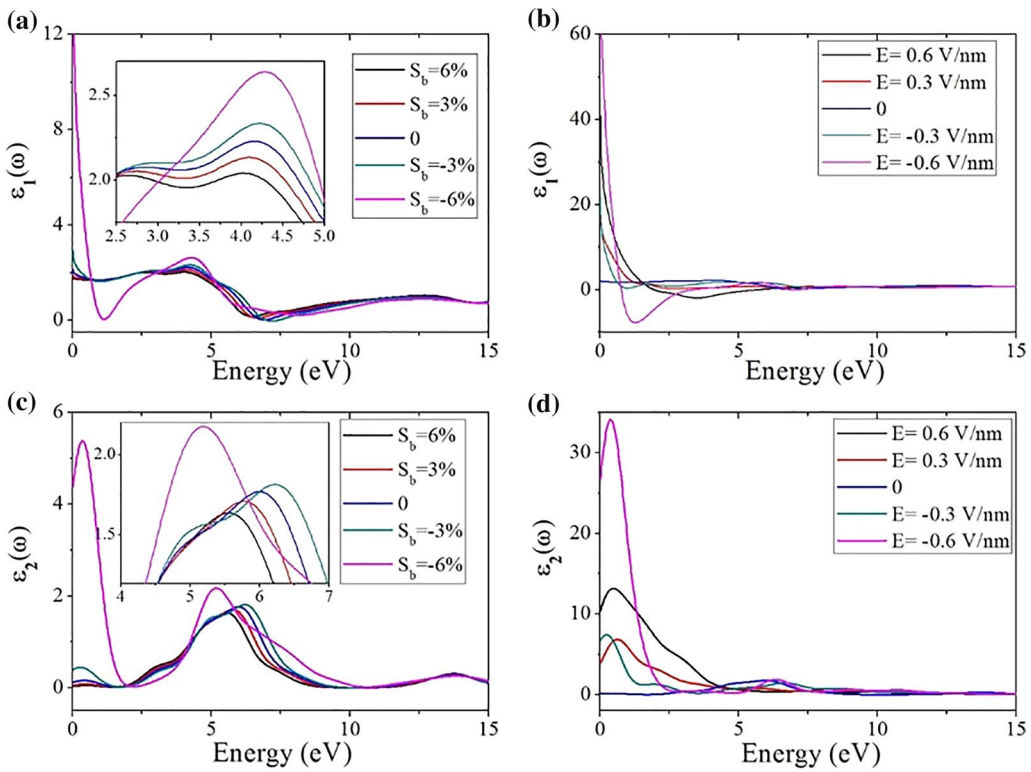

Fig. 8 Calculated parts of dielectric functions of the CsTe monolayer under biaxial strain S_b (a, c) and external electric field (b, d).

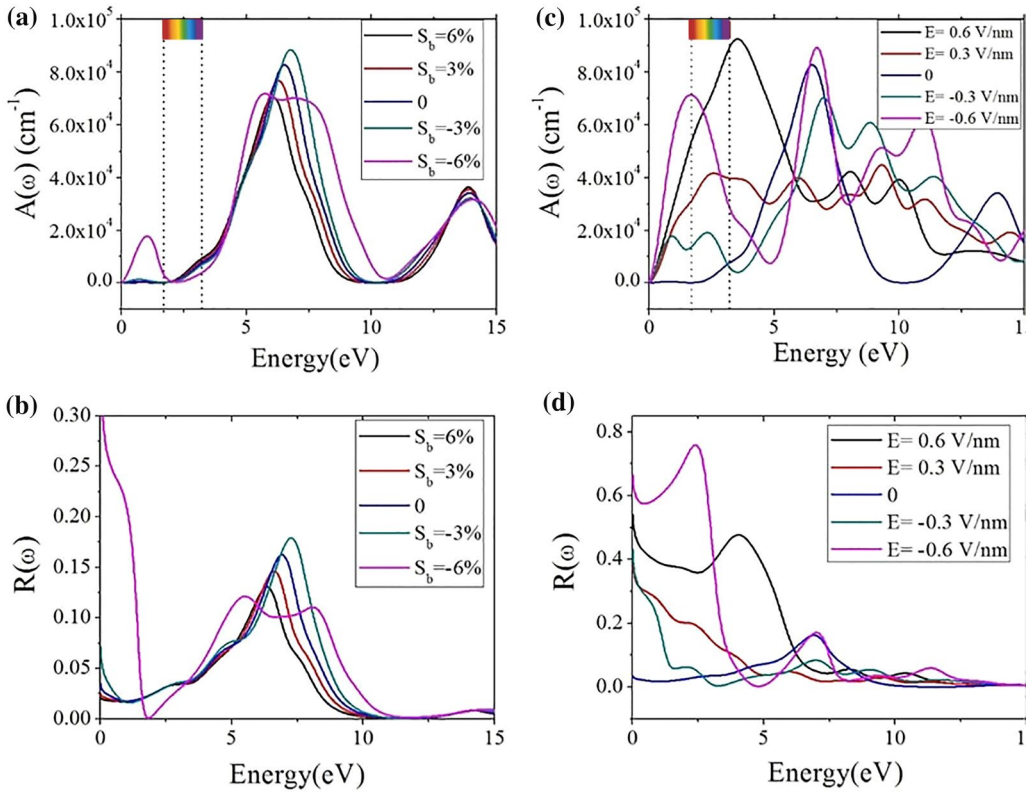

Fig. 9 (a, c) Absorption coefficient $A(\omega)$ under biaxial strain S_b (left) and electric field E (right). (b, d) Optical reflectivity $R(\omega)$ of CsTe monolayer under biaxial strain S_b (left) and electric field E (right).

Funding No funding provided by Basrah University.

Conflict of interest The authors declare that they have no conflict of interest.

References

1. S.A. Wolf, D.D. Awschalom, R.A. Buhrman, J.M. Daughton, S. von Molnar, M.L. Roukes, A.Y. Chtchelkanova, and D.M. Treger, Spintronics: a spin-based electronics vision for the future. *Science* 294, 1488 (2001).
2. J. Zutic, and S.S. Fabian, Sarma, spintronics: fundamentals and applications. *Rev. Mod. Phys.* 76, 323 (2004).
3. C. Felser, G.H. Fecher, and B. Balke, Spintronics: a challenge for materials science and solid-state chemistry. *Angew. Chem. Int. Ed* 46, 668 (2007).
4. R.A. de Groot, F.M. Mueller, P.G. van Engen, and K.H.J. Buschow, New class of materials: half-metallic ferromagnets. *Phys. Rev. Lett.* 50, 2024 (1983).
5. V. Alijani, J. Winterlik, G.H. Fecher, S.S. Naghavi, and C. Felser, Quaternary half-metallic Heusler ferromagnets for spintronics applications. *Phys. Rev. B* 83, 184428 (2011).
6. W.-H. Xie, B.-G. Liu, and D.G. Pettifor, Half-metallic ferromagnetism in transition metal pnictides and chalcogenides with wurtzite structure. *Phys. Rev. B* 68, 134407 (2003).
7. K.I. Kobayashi, T. Kimura, H. Sawada, K. Terakura, and Y. Tokura, Room-temperature magnetoresistance in an oxide material with an ordered double-perovskite structure. *Nature (London)* 395, 677 (1998).
8. K. Schwarz, CrO_2 predicted as a half-metallic ferromagnet. *J. Phys. F: Met. Phys.* 16, L211 (1986).
9. Y.S. Dedkov, U. Rüdiger, and G. Güntherodt, Evidence for the half-metallic ferromagnetic state of Fe3O4 by spin-resolved photoelectron spectroscopy. *Phys. Rev. B* 65, 064417 (2002).
10. Y. Ji, G.J. Strijkers, F.Y. Yang, C.L. Chien, J.M. Byers, A. Anguelouch, G. Xiao, and A. Gupta, Determination of the spin polarization of half-metallic CrO_2 by point contact Andreev reflection. *Phys. Rev. Lett.* 86, 5585 (2001).
11. R. Meservey, and P.M. Tedrow, Spin-polarized electron tunneling. *Phys. Rep.* 238, 173 (1994).
12. R.J. Soulen Jr., J.M. Byers, M.S. Osofsky, B. Nadgorny, T. Ambrose, S.F. Cheng, P.R. Broussard, C.T. Tanaka, J. Nowak, J.S. Moodera, A. Barry, and J.M.D. Coey, Measuring the spin polarization of a metal with a superconducting point contact. *Science* 282, 85 (1998).
13. K.S. Novoselov, A.K. Geim, S.V. Morozov, D. Jiang, Y. Zhang, S.V. Dubonos, I.V. Grigorieva, and A.A. Firsov, Electric field effect in atomically thin carbon films. *Science* 306, 666 (2004).
14. W. Li, L. Kong, C. Chen, J. Gou, S. Sheng, W. Zhang, H. Li, L. Chen, P. Cheng, and K. Wu, Experimental realization of honeycomb borophene. *Sci. Bull.* 63, 282 (2018).
15. C. Jin, F. Lin, K. Suenaga, and S. Iijima, Fabrication of a freestanding boron nitride single layer and its defect assignments. *Phys. Rev. Lett.* 102, 195505 (2009).
16. Q.H. Wang, K. Kalantar-Zadeh, A. Kis, J.N. Coleman, and M.S. Strano, Electronics and optoelectronics of two-dimensional transition metal dichalcogenides. *Nat. Nanotech.* 7, 699 (2012).
17. T. Cao, Z. Li, and S.G. Louie, Tunable magnetism and half-metallicity in hole-doped monolayer GaSe. *Phys. Rev. Lett.* 114, 236602 (2015).

18. Y. Deng, Y. Yu, Y. Song, J. Zhang, N.Z. Wang, Z. Sun, Y. Yi, Y.Z. Wu, S. Wu, J. Zhu, J. Wang, X. Hui, and C.Y. Zhang, Gate-tunable room-temperature ferromagnetism in two-dimensional Fe_3GeTe_2. *Nature (London)* 563, 94 (2018).
19. Z. Fei, B. Huang, P. Malinowski, W. Wang, T. Song, J. Sanchez, W. Yao, D. Xiao, X. Zhu, A.F. May, W. Wu, D.H. Cobden, J.-H. Chu, and X. Xu, Two-dimensional itinerant ferromagnetism in atomically thin Fe_3GeTe_2. *Nat. Mater.* 17, 778 (2018).
20. M. Bonilla, S. Kolekar, Y. Ma, H.C. Diaz, V. Kalappattil, R. Das, T. Eggers, H.R. Gutierrez, M.-H. Phan, and M. Batzill, Strong room-temperature ferromagnetism in VSe_2 monolayers on van der Waals substrates. *Nat. Nanotechnol.* 13, 289 (2018).
21. W. Yu, J. Li, T.S. Herng, Z. Wang, X. Zhao, X. Chi, W. Fu, I. Abdelwahab, J. Zhou, J. Dan, Z. Chen, Z. Chen, Z. Li, J. Lu, S.J. Pennycook, Y.P. Feng, J. Ding, and K.P. Loh, Chemically exfoliated VSe_2 monolayers with room-temperature ferromagnetism. *Adv. Mater.* 31, 1903779 (2019).
22. S. Barua, M.C. Hatnean, M.R. Lees, and G. Balakrishnan, Signatures of the Kondo effect in VSe_2. *Sci. Rep.* 7, 10964 (2017).
23. C. van Bruggen, and C. Haas, Magnetic susceptibility and electrical properties of VSe_2 single crystals. *Solid State Commun.* 20, 251 (1976).
24. A. Mogulkoc, M. Modarresi, and A.N. Rudenko, Two-dimensional chromium pnictides CrX (X = P, As, Sb): Half-metallic ferromagnets with high Curie temperature. *Phys. Rev. B.* 102, 024441 (2020).
25. A. Bafekry, B. Mortazavic, and S. Farjami Shayesteh, Band gap and magnetism engineering in Dirac half-metallic Na_2C nanosheet via layer thickness, strain and point defects. *J. Magn. Magn. Mater.* 491, 165565 (2019).
26. Z. Liu, J. Liu, and J. Zhao, YN_2 monolayer: Novel p-state Dirac half metal for high-speed spintronics. *Nano Res.* 10, 1972 (2017).
27. S. Wang, H. Tian, C. Ren, J. Yu, and M. Sun, Electronic and optical properties of heterostructures based on transition metal dichalcogenides and graphene-like zinc oxide. *Sci. Rep.* 8, 12009 (2018).
28. K. Hoang, S.D. Mahanti, and M.G. Kanatzidis, Impurity clustering and impurity-induced bands in PbTe-, SnTe-, and GeTe-based bulk thermoelectrics. *Phys. Rev. B.* 81, 115106 (2010).
29. K. Hoang, and S.D. Mahanti, Electronic structure of Ga-, In-, and Tl-doped PbTe: a supercell study of the impurity bands. *Phys. Rev. B.* 78, 085111 (2008).
30. K. Hoang, S.D. Mahanti, and P. Jena, Theoretical study of deep-defect states in bulk PbTe and in thin films. *Phys. Rev. B* 76, 115432 (2007).
31. S. Wang, F.R. Pratama, M.S. Ukhtary, and R. Saito, Independent degrees of freedom in two-dimensional materials. *Phys. Rev. B* 101, 081414 (2020).
32. S. Wang, C. Ren, Y. Li, H. Tian, W. Lu, and M. Sun, Spin and valley filter across line defect in silicone. *Appl. Phys. Express* 11, 053004 (2018).
33. W. Sa-Ke, T.H. Yu, Y.Y. Hong, and W. Jun, Spin and valley half metal induced by staggered potential and magnetization in silicone. *Chin. Phys. B.* 23, 017203 (2014).
34. S. Wang, M.S. Ukhtary, and R. Saito, Strain effect on circularly polarized electroluminescence in transition metal dichalcogenides. *Phys. Rev. Res.* 2, 033340 (2020).
35. S. Wang, and J. Yu, Band gap modulation of partially chlorinated graphene (C_4Cl) nanosheets via biaxial strain and external electric field a computational study. *Appl. Phys. A.* 124, 487 (2018).
36. S. Wang, and J. Yu, Tuning electronic properties of silicate layers by tensile strain and external electric field: a first-principles study. *Thin Solid Films* 654, 107 (2018).
37. J.M.K. Al-zyadi, G.Y. Gao, and K.L. Yao, First-principle study of half-metallicity at the TiPo (001) surface and the TiPo/CdTe (001). *Thin Solid Films* 531, 266 (2013).
38. J.M.K. Al-zyadi, R.M. Samuel, G.Y. Gao, and K.L. Yao, The half-metallic characteristics of the (001) surface of zinc-blende TiTe. *J. Magn. Magn. Mater.* 346, 166 (2013).
39. J.M.K. Al-zyadi, N.H. Abdul-Wahhab, and K.L. Yao, Half-metallicity of (001), (110) and (111) surfaces of zinc-blende MnBi and their interfaces with HgTe: a first-principle investigation. *J. Magn. Magn. Mater.* 446, 221 (2018).
40. G.Y. Gao, W. Yao, H.P. Han, J.M.K. Al-zyadi, and K.L. Yao, Stability and half-metallicity of the (001) and (111) surfaces of CrTe with rocksalt structure. *J. Appl. Phys.* 112, 103709 (2012).
41. J.M.K. Al-zyadi, A.H. Ati, and K.L. Yao, First-principles study of half-metallicity bulk rocksalt structure of CsTe and its surfaces. *J. Electron Spectrosc. Relat. Phenom.* 244, 146991 (2020).
42. S.J. Clark, M.D. Segall, C.J. Pickard, P.J. Hasnip, M.I. Probert, K. Refson, and M.C. Payne, First principles methods using CASTEP. *Z. Kristallogr. Cryst. Mater.* 220, 567 (2005).
43. J.P. Perdew, K. Burke, and M. Ernzerhof, Generalized gradient approximation made simple. *Phys. Rev. Lett.* 77, 3865 (1996).
44. S. Wang, and J. Yu, Magnetic behaviors of 3d transition metal-doped silicane: a first-principle study. *J. Supercond. Nov. Magn.* 31, 2789 (2018).
45. R. Dalven, Empirical relation between energy gap and lattice constant in cubic semiconductors. *Phys. Rev. B* 8, 6033 (1973).
46. M. Gajdoš, K. Hummer, G. Kresse, J. Furthmüller, and F. Bechstedt, Linear optical properties in the projector-augmented wave methodology. *Phys. Rev. B* 73, 045112 (2006).
47. G.Y. Guo, K.C. Chu, D.S. Wang, and C.G. Duan, Linear and nonlinear optical properties of carbon nanotubes from first-principles calculations. *Phys. Rev. B* 69, 205416 (2004).